AGU PUBLICATIONS

Earth and Space Science

TECHNICAL REPORTS: METHODS
10.1002/2014EA000023

Key Points:
- A new method is introduced to estimate the Ti content of the Moon's soil
- The lowest reflectance values (R_{min}) are calculated for Sinus Iridum
- Rmin and TiO_2 (0.812) correlation can be used by IIM hyperspectral data

Correspondence to:
L. Li,
liuli@cugb.edu.cn

Citation:
Tingyan X., L. Fujiang, L. Li, L. Chan, Z. Ying, Q. Le, Y. Rong, Z. Xiaopo, Z. Meng, and Z. Qi (2015) Prognosis of Ti abundance in Sinus Iridum using a nonlinear analysis of Chang' E-1 Interference Imaging Spectrometer imagery, *Earth and Space Science*, *2*, 187–193, doi:10.1002/2014EA000023.

Received 1 OCT 2014
Accepted 4 FEB 2015
Accepted article online 13 FEB 2015
Published online 8 MAY 2015

Prognosis of Ti abundance in Sinus Iridum using a nonlinear analysis of Chang' E-1 Interference Imaging Spectrometer imagery

Xing Tingyan[1], Liu Fujiang[2], Liu Li[1], Li Chan[2], Zhang Ying[2], Qiao Le[2], Yang Rong[2], Zheng Xiaopo[2], Zhu Meng[2], and Zhang Qi[2]

[1]Faculty of Information Engineering, China University of Geosciences, Beijing, China, [2]Faculty of Information Engineering, China University of Geosciences, Wuhan, China

Abstract We report here on the relationship between titanium abundance and its spectral features on the Moon, using 36 craters exposed in Sinus Iridum, a landing site for China's Lunar Exploration Program. Six absorption parameters (full width at half maximum, absorption depth (D), absorption position (λ), absorption area (A), absorption asymmetry (S), and (R_{min})) at the wavelength of 500–550 nm were computed, and the lowest reflectance values (R_{min}) to characterize the properties of titanium abundance and its spectral features were calculated. The correlation between R_{min} and TiO_2 abundance calculated by Clementine multispectral images is 0.812, and a second-order polynomial fits the data better with a correlation of 0.837. The TiO_2 abundance inversed by the Chang' E-1 Interference Imaging Spectrometers (IIM) data is thus relatively higher than that revealed by the Clementine data. This good correlation between R_{min} and TiO_2 abundance may thus be used very effectively to estimate the Ti distribution on the surface of the Moon by IIM hyperspectral data.

1. Introduction

The chemical composition of the Moon is fundamental to our understanding of how the Moon was formed, and hence, measurement of its chemical makeup is an important scientific objective for lunar exploration [*Wu et al.,* 2012]. Mapping out the abundance and distribution of Fe and Ti on the surface of the Moon is particularly useful to determine its chemical composition. Lunar Ti characterization is also an important goal of the China Lunar Exploration Program.

The chemistry of lunar soils, such as titanium abundance, has a distinct effect on the spectral characters of the reflected spectrum. On the contrary, we can estimate the titanium abundance based on the spectral characters. Lunar UV/VIS (ultraviolet/visible)-near-infrared spectroscopy has been widely used in lunar geological of studies since the 1970s [*Ling et al.,* 2011], and several sophisticated methods have been developed in recent years.

In this paper, we present a new method to estimate titanium content by Chang' E-1 (CE-1) Interference Imaging Spectrometer (IIM) that uses absorption features of titanium as variables and TiO_2 content measured through sample return of Apollo as dependent variables to make a multiple linear regression. Our results show the existence of a relationship between R_{min} and TiO_2 abundance that in turn can be used effectively to estimate the compositional variations on the Moon's surface more precisely than the other, recently introduced techniques. Our method can also be applied in the elemental and resource mapping and spectral studies of some regions on the Earth where mafic-ultramafic rocks with significant variations in Ti contents exist in large-scale continental intrusions and ophiolites. In the first part of the paper we briefly discuss the previous work and methods by other researchers and evaluate their significance. We then introduce our database, method, and TiO_2 quantitative inversion model. In the last part of the paper, we discuss the results of our hyperspectral data-based observations and results for more precise estimation of TiO_2 distribution in lunar soil in comparison to other widely used methods. We also briefly discuss the implications of space weathering effects on soil and regolith compositions on planetary surfaces for our method.

2. Previous Work

The global maps of the FeO and TiO_2 contents of the lunar surface have been made previously, based on Clementine UV/VIS images and data [*Lucey et al.,* 1995, 1998; *Shkuratov et al.,* 1999, 2005; *Korokhin et al.,* 2008;

Table 1. Parameters of CE-1's IIM Instrument

Parameters	Values
Image width	25.6 km
Image coverage	75°N–75°S (when Sun elevation angle > 15°)
Pixel resolution	200 m (subastral point)
Spectral coverage	480 nm to 960 nm
Bands and spectral resolution	32 (9.6 nm@543.5 nm, 13.1 nm@632.8 nm, 20 nm@783.8 nm, 22.5 nm@831.2 nm)
Radiation resolution/bit	12 bits
S/N	≥100 (r = 0.2, solar incidence angle = 30°)

Wöhler et al., 2011]. Using lunar data, *Lucey et al.* [1998, 2000] presented new methods to estimate the Ti content based on Clementine UV-VIS imagery, whereby the Ti-sensitive optical parameters is as follows:

$$\theta_{\mathrm{Ti}} = \arctan\left(\frac{R_{415}/R_{750} - E}{R_{750} - F}\right) \quad (1)$$

where R_{415} and R_{750} are reflectance values at 415 nm and 750 nm and E and F are the UV/VIS ratio and 750 nm reflectance of the optimized origin, respectively. Then, using two different sets of modified regression parameters for calculating TiO_2, *Gillis et al.* [2003] proposed a revised algorithm based on the work of *Lucey et al.* [2000]. Subsequently, the same researchers [*Gillis et al.,* 2006] used the correlation between TiO_2 and UV/VIS color to explain the ilmenite/TiO_2 content of the lunar maria.

Recently, some studies have utilized Chang' E-1 data in order to improve the usability of IIM data. *Wu et al.* [2012] proposed a preprocessing method of CE-1 IIM data, including calibration and flat-field correction, and mapped the global distribution of FeO and TiO_2 [*Wu et al.,* 2009, 2010]. *Liu et al.* [2010] used absorption features of titanium as variables and TiO_2 content measured through Apollo sample as dependent variables to build a multiple linear regression by CE-1 Interference Imaging Spectrometer (IIM) that are as follows:

$$\mathrm{TiO_2}\% = -0.3227 \times W + 13.4422 \times D + 0.1755 \times \lambda + 0.9440 \times A + 5.8412 \times S - 85.9416 \quad (2)$$

$$\mathrm{TiO_2}\% = 149.6413 \times D - 0.0223 \times \lambda - 2.9757 \times A + 7.0842 \times S + 11.8631 \quad (3)$$

where W is the full wave at half maximum (FWHM), λ is the absorption position, D is the absorption depth, A is the absorption area, and S is the absorption asymmetry.

More recently, *Ling et al.* [2011] applied a preliminary algorithm based on "ground truths" from Apollo and Luna sample return sites for mapping titanium abundance from IIM image. *Wang and Niu* [2012] have established the spectral parameters that possess good nonlinear correlations with lunar titanium abundance by using samples from Apollo and Luna landing sites. They estimated lunar titanium abundance using a Decision Tree Method C5.0-Support Vector Machine method.

3. Interference Imaging Spectrometer Data

Interference Imaging Spectrometer (IIM) was boarded on CE-1 and launched on 24 October 2007 by Chinese National Space Administration. Hyperspectral images with 32 bands, a ground resolution of 200 m, and wavelength range of 480–960 nm have been obtained. IIM is the first sensor to map the Moon using interference technology hyperspectrally, which provides a powerful way to derive the compositions of the lunar surface. The instrument parameters of IIM are listed in Table 1, and the additional information can be obtained from Ground Application System of Lunar Exploration in the National Astronomical Observatories at the Chinese Academy of Sciences (http:// bao.ac.cn/).

Table 2 lists the landing sites and TiO_2 abundance of Apollo 11, 12, and 14–17 [*Blewett et al.,* 1997; *Lucey et al.,* 2000; *Jolliff,* 1999]. It is known that lunar sample 62231 collected by Apollo 16 has been used as a representative of lunar soil compositions and as the standard to calibrate image data. In this paper, to compare with TiO_2 abundance estimated from sample return spectra of Apollo that measured by Reflectance Experiment Laboratory (RELAB) of Brown University, IIM images were calibrated to sample 62231.

4. Methods

4.1. Calibration and Noise Reduction

Ground Control Points (GCPs) can be found in the header of IIM data, and the imagery has been radiometrically and photometrically calibrated, and georegistered with a RMS less than 0.21. However, serious noise still

Table 2. Coordinates and Soil Compositions of the Landing Sites

Site	Latitude (deg)	Longitude (deg)	TiO_2 (wt %)	Site	Latitude (deg)	Longitude (deg)	TiO_2 (wt %)
Apollo 11	0.725	23.487	7.5	Apollo 16-S13	−8.830	15.522	0.5
Apollo 12	−2.989	336.687	3.1	Apollo 17-LM	20.192	30.742	8.5
Apollo 14-LM	−3.673	342.604	1.73	Apollo 17-S1	20.156	30.753	9.6
Apollo14-Cone	−3.656	342.646	1.6	Apollo 17-S2	20.096	30.496	1.5
Apollo15-LM	26.138	3.674	1.9	Apollo 17-S3	20.170	30.534	1.8
Apollo15-S1	26.034	3.643	1.6	Apollo 17-S5	20.186	30.694	9.9
Apollo15-S2	26.013	3.626	1.3	Apollo 17-S6	20.289	30.771	3.4
Apollo15-S4	26.036	3.701	1.2	Apollo 17-S7	20.291	30.784	3.9
Apollo15-S6	25.978	3.720	1.5	Apollo 17-S8	20.280	30.849	4.3
Apollo15-S7	25.990	3.706	1.1	Apollo 17-S9	20.226	30.802	6.4
Apollo15-S8	26.142	3.670	1.7	Apollo 17-LRV1	20.176	30.654	8.0
Apollo15-S9	26.138	3.611	1.8	Apollo 17-LRV2	20.180	30.617	4.4
Apollo15-S9a	26.138	3.604	2.0	Apollo 17-LRV3	20.183	30.596	5.5
Apollo16-LM	−8.955	15.511	0.6	Apollo17-LRV4/S2a	20.108	30.516	1.3
Apollo 16-S1	−8.955	15.462	0.6	Apollo 17-LRV5	20.185	30.556	2.6
Apollo 16-S2	−8.895	15.480	0.6	Apollo 17-LRV6	20.194	30.565	2.6
Apollo 16-S4	−9.080	15.509	0.5	Apollo 17-LRV7	20.216	30.633	6.8
Apollo 16-S5	−9.059	15.515	0.7	Apollo 17-LRV8	20.205	30.662	6.6
Apollo 16-S6	−0.955	15.500	0.7	Apollo 17-LRV9	20.233	30.749	6.1
Apollo 16-S8	−9.043	15.480	0.6	Apollo17-LRV10	20.283	30.755	3.7
Apollo 16-S9	−9.035	15.491	0.6	Apollo17-LRV11	20.276	30.841	4.5
Apollo 16-S11	−8.805	15.513	0.4	Apollo17-LRV12	20.198	30.781	10.0

exists, especially at first several and last two bands. In order to suppress the noise and stripes we first performed Minimum Noise Fraction (MNF) transformation and then inverse-MNF transformation. MNF and inverse-MNF are generally used to reduce hyperspectral image noise [*Liu et al.,* 2010]. The MNF sequentially performs two principle component analyses on the data: the first separates white noise, i.e., uninformative data, and the second recombines these bands into new composite bands, which account for most of the variance in the original data (informative data) [*Underwood et al.,* 2003]. After MNF processing (following MNF), an eigenvectors graph is prepared, wherein the values represent variance of every MNF component. Based on this graph, the first eight MNF components were selected to perform inverse MNF to regain the original images. Noise and stripe were significantly reduced, and spectra were pronounced improved.

Zigzag noise appears on the spectra of IIM images due to the low spectral resolution (see Table 1). To weaken the zigzag, IIM spectra were primo resampled to RELAB spectra with a sample interval at 5 nm, allowing the Empirical Flat Field Optimal Reflectance Transformation (EFFORT) to work efficiently. EFFORT searches for a mild linear correction, bootstrapped from the data themselves that polish out this error and attempts to improve the accuracy of the apparent reflectance data [*Boardman,* 1998]. After an EFFORT performance, the spectra appear smooth and more like spectra of real materials. The spectra before and after the EFFORT performance are greatly different.

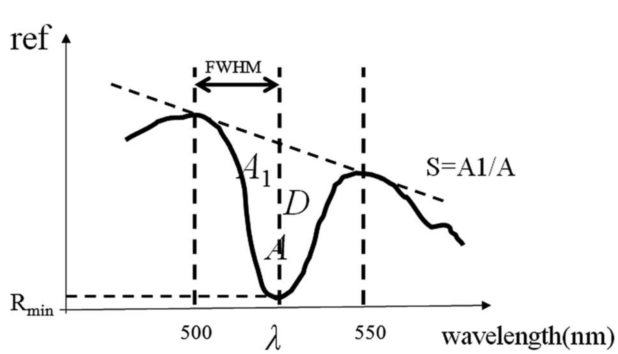

Figure 1. Diagram of the absorption parameters.

4.2. Spectral Absorption Features

Spectral reflectance in the visible and near-infrared wavelengths provides a rapid and inexpensive means for determining the mineralogy of samples and for obtaining information on chemical composition. Spectral absorption features parameters such as the position, depth, width, and asymmetry of the feature have been used to quantitatively estimate sample compositions from hyperspectral field and laboratory reflectance data. The parameters have also been used to develop mapping methods for

Table 3. Values of Six Absorption Parameters for Apollo 17 and the Correlation Coefficient Between Ti Content and Each Absorption Parameter

No.	FWHM (*W*)	Absorption Depth (*D*)	Absorption Position (λ)	Absorption Area (*A*)	Absorption Asymmetry (*S*)	Lowest Reflectance (R_{min})
LM	27.5	0.0302	520	1.3783	0.5571	8.5
S2	15	0.0063	505	0.2936	0.2024	1.5
S3	17.5	0.0085	505	0.3353	0.1951	1.8
S5	30	0.0287	525	1.5649	0.8435	9.9
S7	27.5	0.0280	520	1.0252	0.3310	3.9
S8	30	0.0173	530	1.0438	1.1322	4.3
LRV1	30	0.0201	525	0.9971	0.8637	8
LRV2	30	0.0181	525	0.8998	0.7969	4.4
LRV3	30	0.0199	505	0.6278	0.0891	5.5
LRV4	30	0.0090	510	0.4336	0.2762	1.3
LRV5	30	0.0141	520	0.7077	0.6862	2.6
LRV6	30	0.0231	525	1.2512	0.9333	2.6
LRV7	15	0.0052	505	0.2774	0.1972	6.8
LRV8	10	0.0150	520	0.4444	3.6070	6.6
LRV9	10	0.0161	520	0.4613	3.5923	6.1
LRV10	30	0.0185	525	0.0108	0.8551	3.7
LRV11	27.5	0.0227	520	1.128	0.5771	4.5
LRV12	25	0.0106	520	0.4718	0.5730	10
Ti	−0.022	0.354	0.305	0.344	0.220	0.823

the analysis of hyperspectral image data [*Van Der Meer,* 2004]. As the charge transfer between Fe-O and Fe-Ti, there exists a distinct spectral absorption band approximately at 550 nm, which lead to the ratio image of UV/VIS become dark and "red." In this study, we computed five absorption parameters, i.e., full wave at half maximum (FWHM), absorption depth (*D*), absorption position (λ), absorption area (*A*), and absorption asymmetry (*S*), at the wavelength of 500–550 nm. In addition, we calculated the lowest reflectance values (R_{min}) among 500 nm to 550 nm. Figure 1 displays a diagram of the five spectral absorption feature parameters and R_{min}.

4.3. Derivation of the TiO_2 Quantitative Inversion Model

From the IIM images we selected the spectra of 21 points (3 × 3 on average each) corresponding to Apollo 17 landing sites to reveal the relationship between the titanium content and its absorption feature. The values of the six spectral absorption feature parameters are listed in Table 3. The correlation coefficients of six absorption parameters and TiO_2 content are listed at the last line of Table 3. As shown in Figure 3, except for lowest reflectance (R_{min}), correlation coefficients of the others are too low, all less than 0.36, whereas the correlation coefficient between lowest reflectance (R_{min}) and TiO_2 content (0.823) is very high. All of the

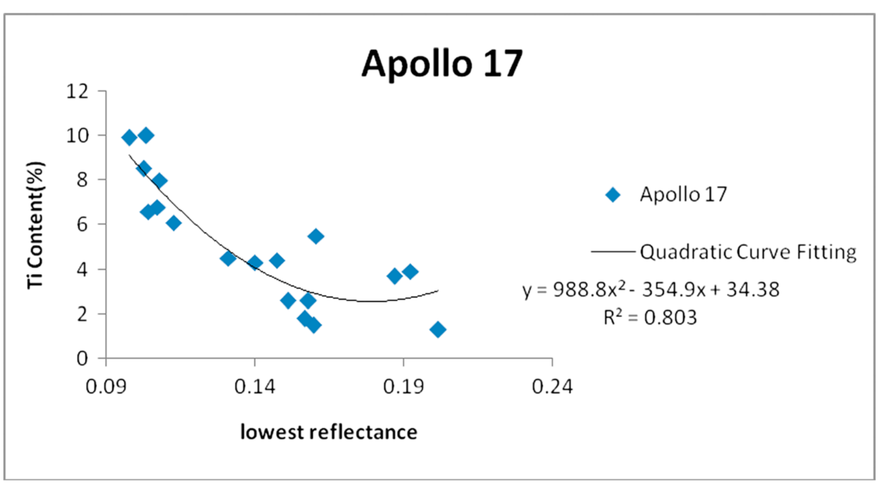

Figure 2. Scatter graph of the lowest reflectance against the Ti content.

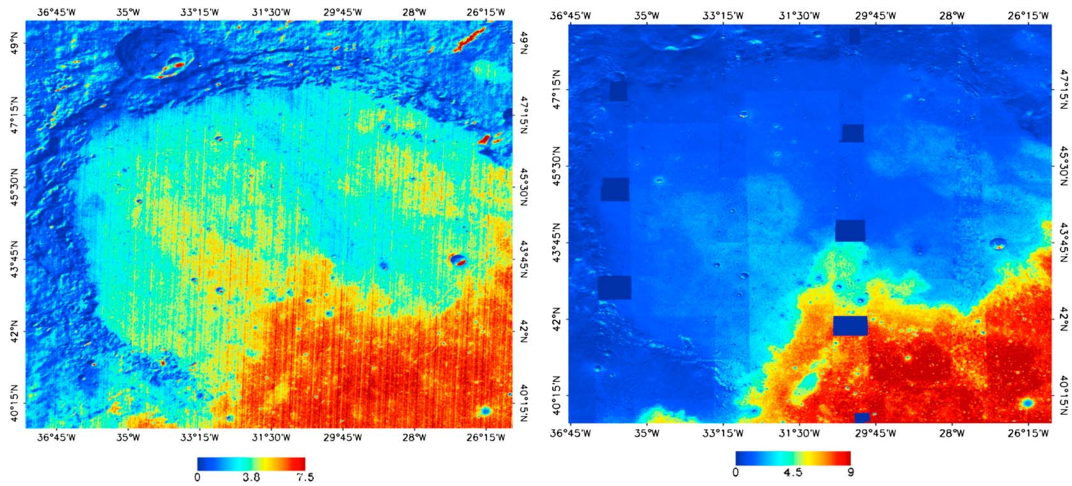

Figure 3. Mapping of TiO_2 abundance at Sinus Iridum based on (left) CE-1 IIM (this study) and (right) Clementine by *Lucey et al.* [2000].

spectral absorption features except R_{min} are very weak and hard to quantify for mature lunar soils because of space weathering effects. The absorption feature of ilmenite is rarely seen in the lunar spectral but only shown by the blue shift of the short wavelengths. This is the reason as to why the five spectral parameters have very poor relation with the Ti content.

According to the principle of correlation coefficient, a relatively low value cannot show any essential relationship between the two discrete variables. On the contrary, the interposition of a variable with low correlation coefficient may disturb the stability of a model and its theoretical feasibility. Therefore, in this study we just analyzed the relationship between the lowest reflectance and TiO_2 content and established a model to prognose titanium content at a larger spatial scale. We make a quadratic curve fitting between R_{min} and TiO_2 content and obtain a nonlinear model equation (4). Figure 2 displays the scatter graphs of the lowest reflectance against the Ti content. The relation coefficient R between equation (4) and 18 points is 0.896. This value is relatively high, but the model can be used to prognose the titanium content.

$$y = 988.8x^2 - 354.9x + 34.38 \quad (4)$$

where x is lowest reflectance (R_{min}) and y is Ti content.

5. Discussion

5.1. Comparative Analysis of Lunar TiO_2 Abundance and its Spectra

We selected 36 craters in Sinus Iridum located in the northwestern of Mare Imbrium to characterize the properties of TiO_2 abundance and its spectra. We mapped the TiO_2 abundance of Sinus Iridum based on the

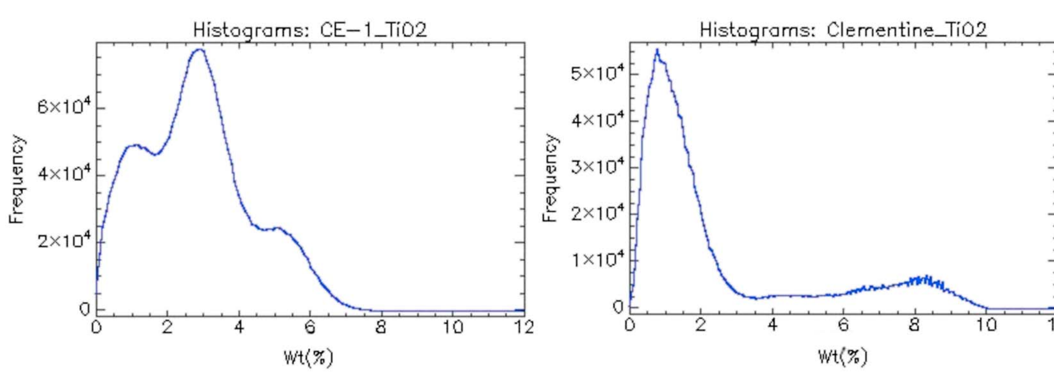

Figure 4. Histograms of the TiO_2 abundance maps at Sinus Iridum based on (left) CE-1 IIM (this study) and (right) the Clementine data by *Lucey et al.* [2000].

Table 4. Lowest Reflectance Values (R_{min}) and the TiO_2 Contents of the 36 Craters at Sinus Iridum

No.	R_{min}	TiO_2	No.	R_{min}	TiO_2	No.	R_{min}	TiO_2
1	0.21807	0.702262	13	0.21243	0.864382	25	0.07924	3.41414
2	0.17086	0.424706	14	0.20732	0.707286	26	0.0821	6.2978
3	0.26576	0.439216	15	0.21379	0.7217	27	0.07102	3.41896
4	0.20288	0.865781	16	0.2302	0.552449	28	0.08306	4.76663
5	0.19746	0.833488	17	0.16939	0.867635	29	0.06965	4.68669
6	0.25083	0.542981	18	0.2191	2.33008	30	0.0766	8.01406
7	0.19357	1.39638	19	0.20963	3.28305	31	0.08112	6.94656
8	0.18253	0.688262	20	0.17402	4.28122	32	0.13622	4.58932
9	0.2098	0.627447	21	0.29006	1.89615	33	0.10414	4.81066
10	0.22706	0.518905	22	0.07454	3.97042	34	0.09437	4.04669
11	0.23473	0.848614	23	0.08306	6.94702	35	0.08066	3.70576
12	0.19847	0.626158	24	0.09295	6.32808	36	0.1008	4.22523

CE-1 IIM data and the Clementine data according to the approach presented by *Lucey et al.* [2000], whereby the error is at a low level of 1–2 wt % [*Xu and Li,* 2001] using Clementine UV/VIS imagery (Figure 3). Both the CE-1 and Clementine images show that the TiO_2 abundance is very low, but the TiO_2 abundance inversed by the CE-1 IIM data is relatively higher than that revealed by the Clementine data. The mean value of TiO_2 abundance is 6.26 wt % and 2.59 wt %, respectively. Figure 4 display histograms of the maps at Sinus Iridum. On the TiO_2 histogram of the CE-1 IIM data we see a trimodal distribution of the main peaks at ~1 wt %, 2.8 wt %, and 5.3 wt %, whereas on the histogram based on the Clementine data we only see a bimodal distribution of the main peaks at 0.9 wt % and 8.1 wt %. In general, the inversion results using our model based on the CE-1 IIM hyperspectral data show a good correlation with multispectral Clementine data. However, we posit that from the point of inversion accuracy aspect, our model of TiO_2 abundance extraction based on CE-1 predicts higher results and better resolution compared to those based on Clementine. Thus, we think that the hyperspectral data based on CE-1 IIM make the observations of TiO_2 distribution in lunar soil more precise than multispectral Clementine data.

Then, five absorption parameters and R_{min} of the 36 craters were worked out by IIM images. We have observed that the correlation between R_{min} and TiO_2 abundance calculated by Clementine multispectral images is 0.812 and that second-order polynomial fits the data better with a correlation of 0.837. The lowest reflectance values and the TiO_2 content of the 36 craters are listed in Table 4.

5.2. Space Weathering Effects

It has been well established that space weathering of planetary surfaces and soils may obscure direct evidence of bedrock crustal compositions [*Hapke*, 2001*; Taylor et al.*, 2001*; Chapman*, 2004*; Noguchi et al.*, 2011] because it may reduce the albedo effect, weaken the spectral absorption features, and redden mineral spectral reflectance due to the presence of nanophase iron particles (np-FeO). Different levels of np-FeO are associated with different space weathering processes, and different space weathering levels are thought to be proportional to np-FeO [*Hapke,* 2001].

Simulating different levels of space weathering effects with optical maturity parameters (i.e., single-scattering albedos, absorption coefficients, and the photon path length), we can select the optimal and closest conditions to establish our inversion model. However, the complex physical, chemical, and mineralogical effects of space weathering on lunar regolith and soil are significantly controlled by equally complex interrelationships among Moon's exospheric processes, the space environment, and surface (crustal bedrock) composition. This topic is outside the scope of our method-based study here, but we are keen to improve our method to further advance the inversion precision. We shall report the outcome of these ongoing efforts elsewhere.

6. Conclusions

This paper focuses on the relationship between titanium abundance and its spectral features in Sinus Iridum in the northwestern part of Mare Imbrium and presents a new method utilizing the IIM data. Our research shows that there is a good correlation between R_{min} and TiO_2 abundance, which can be used to estimate TiO_2 abundance by IIM hyperspectral data. Furthermore, the TiO_2 abundance inversed by the CE-1 IIM data is relatively higher than that revealed by the Clementine data, indicating that the results of our method appear to be more precise than those based on multispectral Clementine data. Our method and its results (particularly the inversion precision) may have, however, some shortcomings because our inversion model does not take into consideration the potential effects of terrain influence and space weathering. We are currently treating these issues and the related boundary conditions in our method to further improve the inversion precision and will report on our results in a future paper.

Acknowledgments
This project was supported by the Research Foundation of Science and Technology, the Fundamental Research Funds for the Central Universities, China University of Geosciences. We are grateful to Xiao Long and Wu Jun for their suggestions. We are also grateful to the National Astronomical Observatories of China for providing the IIM data and to Wu Yunzhao for providing us with the approach to calibrate IIM spectra to the spectra of sample return 62231, to the USGS and NASA where Clementine data can be downloaded for free, and to RELAB of Brown University who provided the spectra of lunar samples. The CE-1 data are available at http://moon.bao.ac.cn/. Apollo samples data can be downloaded from the website http://www.planetary.brown.edu/relabdocs/. Additional instructions for accessing these data can be obtained from Liu Li (liuli@cugb.edu.cn). Constructive and detailed comments by three anonymous referees and Editor J. Jiang helped us improve the science and organization in the manuscript, and we gratefully acknowledge them.

References

Blewett, D. T., P. G. Lucey, B. R. Hawke, and B. L. Jolliff (1997), Clementine images of the lunar sample-return stations: Refinement of FeO and TiO_2 mapping techniques, *J. Geophys. Res.*, *102*(E7), 16,319–16,325, doi:10.1029/97JE01505.

Boardman, J. W. (1998), Post-ATREM polishing of AVIRIS apparent reflectance data using EFFORT: A lesson in accuracy versus precision, in *Summaries of the Seventh JPL Airborne Earth Science Workshop*, JPL Publication 97-21, vol. 1, pp. 53, Jet Propul. Lab., California Institute of Technology, Pasadena, Calif.

Chapman, C. R., (2004), Space weathering of asteroid surfaces, *Annu. Rev. Earth Planet. Sci.*, *32*, 539–567.

Gillis, J. J., B. L. Jolliff, and R. C. Elphic (2003), A revised algorithm for calculating TiO_2 from Clementine UVVIS data: A synthesis of rock, soil, and remotely sensed TiO_2 concentrations, *J. Geophys. Res.*, *108*(E2), 5009, doi:10.1029/2001JE001515.

Gillis, J. J., P. G. Lucey, and B. Hawke (2006), Testing the relation between UV-vis color and TiO_2 content of the lunar maria, *Geochim. Cosmochim. Acta*, *70*, 6079–6102.

Hapke, B. (2001), Space weathering from Mercury to the asteroid belt, *J. Geophys. Res.*, *106*(E5), 10,039–10,073, doi:10.1029/2000JE001338.

Jolliff, B. L. (1999), Clementine UV/VIS multispectral data and the Apollo 17 landing site: What can we tell and how well?, *J. Geophys. Res.*, *104*(E6), 14,123–14,148, doi:10.1029/1999JE900012.

Korokhin, V. V., V. G. Kaydash, Y. G. Shkuratov, D. G. Stankevich, and U. Mall (2008), Prognosis of TiO_2 abundance in lunar soil using a non-linear analysis of Clementine and LSCC data, *Planet. Space Sci.*, *56*(8), 1063–1078.

Ling, Z. C., J. Zhang, J. Z. Liu, W. X. Zhang, W. Bian, X. Ren, LingLi M., J. J. Liu and C. L. Li (2011), Preliminary results of FeO mapping using Imaging Interferometer data from Chang'E-1, *Chin. Sci. Bull.*, *56*(4–5), 376–379.

Liu, F. J., L. Qiao, Z. Liu, R. Yang, J. P. Shi, Y. Zhang, and W. Wu (2010), Estimation of lunar titanium content: Based on absorption features of Chang'E-1 interference imaging spectrometer (IIM), *Sci. China: Phys., Mech. Astron.*, *53*(12), 2136–2144.

Lucey, P. G., G. J. Taylor, and E. Malaret (1995), Abundance and distribution of iron on the Moon, *Science*, *268*(5214), 1150–1153.

Lucey, P. G., D. T. Blewett, and B. R. Hawke (1998), Mapping the FeO and TiO_2 content of the lunar surface with multispectral imagery, *J. Geophys. Res.*, *103*(E2), 3679–3699, doi:10.1029/97JE03019.

Lucey, P. G., D. T. Blewett, and B. L. Jolliff (2000), Lunar iron and titanium abundance algorithms based on final processing of Clementine ultraviolet-visible images, *J. Geophys. Res.*, *105*(E8), 20,297–20,305, doi:10.1029/1999JE001117.

Noguchi, T., et al. (2011), Incipient space weathering observed on the surface of Itokawa dust particles, *Science, 333*(6046), 1121–1125, doi:10.1126/science.1207794.

Shkuratov, Y. G., V. G. Kaydash, and N. V. Opanasenko (1999), Iron and titanium abundance and maturity degree distribution on the lunar nearside, *Icarus*, *137*(2), 222–234.

Shkuratov, Y. G., V. G. Kaydash, D. G. Stankevich, L. V. Starukhina, P. C. Pinet, S. D. Chevrel, and Y. H. Daydou (2005), Derivation of elemental abundance maps at intermediate resolution from optical interpolation of lunar prospector gamma-ray spectrometer data, *Planet. Space Sci.*, *53*(12), 1287–1301.

Taylor, L. A., C. M. Pieters, L. P. Keller, R. V. Morris, and D. S. McKay (2001), Lunar mare soils: Space weathering and the major effects of surface-correlated nanophase Fe, *J. Geophys. Res.*, *106*, 27,985–27,999, doi:10.1029/2000JE001402.

Underwood, E., S. Ustin, and D. DiPietro (2003), Mapping nonnative plants using hyperspectral imagery, *Remote Sens. Environ.*, *86*(2), 150–161.

Van Der Meer, F. (2004), Analysis of spectral absorption features in hyperspectral imagery, *Int. J. Appl. Earth Obs. Geoinf.*, *5*(1), 55–68.

Wang, X. M., and R. Q. Niu (2012), Lunar titanium abundance characterization using Chang'E-1 IIM data*, Sci. China: Phys., Mech. Astron.*, *55*(1), 170–178.

Wöhler, C., A. Berezhnoy, and R. Evans (2011), Estimation of elemental abundances of the lunar regolith using Clementine UVVIS+ NIR data, *Planet. Space Sci.*, *59*(1), 92–110.

Wu, Y. Z., X. S. Xu, Z. D. Xie, and Z. S. Tang (2009), Absolute calibration of the Chang'E-1 IIM camera and its preliminary application*, Sci. China, Ser. G: Phys., Mech. Astron.*, *52*(12), 1842–1848.

Wu, Y. Z., B. Xue, B. Zhao, P. Lucey, J. Chen, X. Xu, C.-L. Li, and Z. Ouyang (2012), Global estimates of lunar iron and titanium contents from the Chang' E-1 IIM data, *J. Geophys. Res.*, *117*, E02001, doi:10.1029/2011JE003879.

Wu, Y., Y. Zheng, Y. Zou, J. Chen, X. Xu, Z. Tang, A. Xu, B. Yan, F. Gan, and X. Zhang (2010), A preliminary experience in the use of Chang'E-1 IIM data, *Planet. Space Sci.*, *58*(14), 1922–1931.

Xu, T., and C. Li (2001), Abundances and distribution of elements on the lunar surface, *Chin. J. Space Sci.*, *21*, 332–340.